Optical Materials 37 (2014) 251–256

Contents lists available at ScienceDirect

Optical Materials

journal homepage: www.elsevier.com/locate/optmat

Luminescence properties of zirconia nanocrystals prepared by solar physical vapor deposition

Krisjanis Smits [a,*], Larisa Grigorjeva [a], Donats Millers [a], Karlis Kundzins [a], Reinis Ignatans [a], Janis Grabis [b], Claude Monty [c]

[a] Institute of Solid State Physics, University of Latvia, Riga, Latvia
[b] Institute of Inorganic Chemistry, Riga Technical University, Latvia
[c] Procédés, Matériaux et Energie Solaire CNRS, France

ARTICLE INFO

Article history:
Received 14 April 2014
Received in revised form 12 May 2014
Accepted 1 June 2014
Available online 26 June 2014

Keywords:
Zirconia
Upconversion luminescence
Biolabeling
Nanocrystals

ABSTRACT

Zirconia nanocrystals have attracted considerable interest as biolabels, which can be used as probes for medical imaging and biosensor applications. However, zirconia particle agglomeration forms a major limitation to its use for biolabeling. In this backdrop, for the first time, well-separated zirconia nanocrystals were obtained in a Heliotron reactor (PROMES CNRS, France) via the solar physical vapor deposition (SPVD) method. As the raw material target for solar evaporation, zirconia nanopowders obtained via the sol–gel process were used. The luminescence and upconversion luminescence properties of the Sol Gel nanopowders were compared with those of the SPVD nanocrystals. Erbium was chosen as the luminescence center with ytterbium as the sensitizer, and along with these two dopants, niobium was also used. Niobium acts as a charge compensator to compensate for depletion in the charge due to the introduction of trivalent erbium and ytterbium at tetravalent zirconium sites. Consequently, the oxygen-vacancy concentration is reduced, and this results in a significant increase in the upconversion luminescence.

The SPVD-prepared samples showed less agglomeration and a fine crystal structure as well as high luminescence, and thus, such samples can be of great interest for biolabeling applications.

1. Introduction

Zirconia (ZrO_2) is considered an excellent material for use in optics due to its wide bandgap, good transparency, and high refractive index and material hardness [1]. On the other hand, the phonon energy of ZrO_2 is low, and therefore, its luminescence thermal quenching is less efficient than in certain other optical materials.

The intrinsic luminescence of zirconia is relatively weak, and therefore, for practical luminescence applications, zirconia is doped with rare earth (RE) ions. The RE-ion luminescence characteristics in zirconia are concentration-dependent, and concentration quenching of RE ions in zirconia nanocrystals can be observed at relatively high concentrations, which indicates that the RE distribution in nanocrystals is homogeneous [2]. The RE-ion luminescence in ZrO_2 depends on its nanocrystal grain size [3]. On the one hand, increase in the grain size reduces the surface defect concentration, thereby reducing the possibility of excitations recombining in a nonradiative manner. On the other hand, an increase in the grain size for doping concentrations less than 3 mol% could lead to the compound's phase transition from tetragonal to monoclinic.

We have recently demonstrated the possibility of using zirconia-nanocrystal upconversion luminescence in biolabeling [4]. Such applications have also been reported by other researchers [5]. Zirconia nanocrystals can be prepared by different chemical methods; however, in most cases, the final products mostly agglomerate even upon using surfactants. However, for biolabeling applications, separated (not agglomerated) nanocrystals are necessary. Our previous study on zirconia powder prepared in plasma [6] resulted in significantly reduced agglomeration. It is expected that similar or better results can be obtained using the SPVD method. Further, the morphology of SVPD-prepared oxide nanocrystals strongly differs from those of samples obtained via the Sol Gel method [7]. In addition, the SPVD sample quantities are smaller in comparison with those obtained via the plasma method. This provides an easy approach to test the differences in composition between the two methods.

* Corresponding author. Tel.: +371 26538386.
E-mail address: smits@cfi.lu.lv (K. Smits).

http://dx.doi.org/10.1016/j.optmat.2014.06.003
0925-3467/

Zirconia nanocrystals are non-toxic (zirconia are often used in biological implants), and therefore, the possible application of zirconia for biolabeling has attracted strong interest. However, the downside of using zirconia in biolabeling is its relatively weak luminescence compared with certain fluorides. Nevertheless, we have recently shown the reason for the decrease in the upconversion luminescence intensity [8] and how this reduction can be avoided by adding Nb dopant [9].

For the upconversion luminescence center, we chose Er ions as the dopants; additional doping with Yb enhances the upconversion process efficiency (due to the large absorption cross-section of the Yb ions) for optical absorption and effective energy transfer to Er ions. Both Er and Yb are incorporated in Zr^{4+} sites as RE^{3+}; therefore, for charge compensation, oxygen vacancies can also be incorporated in zirconia. As assumed by Fabris et al. [10], oxygen vacancies stabilize tetragonal or even cubic zirconia phases; however, oxygen vacancies could affect the energy transfer from one RE ion to another.

Our previous researches show the possibility of varying the oxygen vacancy concentration in zirconia [6,8] thereby allowing for the examination of the influence of oxygen vacancies on the luminescence properties. Another possible method to vary the vacancy concentration in zirconia doped with trivalent dopants is to add Nb^{5+} [11–13], which also leads to increase of dopant luminescence [9].

In this article, we describe our investigation of the luminescence properties of Er-, Yb- and Nb-doped zirconia nanocrystal samples prepared via SPVD and our comparison of these properties with those of nanocrystals prepared via the classical Sol Gel method.

2. Experimental

2.1. Sample preparation

Erbium-, ytterbium-, and niobium-doped zirconia samples were prepared by the Sol Gel and SVPD methods. Further, samples with only Er and Yb (without Nb) were also prepared for purposes of comparison in the backdrop of our previous research that describes the role of Nb in luminescence increase [9]. This study focuses mainly on Nb-doped samples. We primarily compare SPVD 12-8 samples with sample Sol Gel 13-8a samples. The sample names and descriptions are listed in Table 1.

Er and Yb concentrations for the Sol Gel method were chosen such that the resulting concentrations for the both the SPVD and Sol Gel samples were identical. The Sol Gel sample synthesis method has been described previously [8,14,15].

The SPVD samples were prepared in a Heliotron reactor (PROMES CNRS) in a manner similar to that described by Kouam et al. [16]. The target pellets for SVPD experiments were synthesized by the Sol Gel method with 1 and 2 mol% of Er and Yb, respectively, and 3 mol% Nb. However, subsequent to SPVD, the Er and Yb amounts in the resulting nanocrystal powder were significantly lower. The Er and Yb quantities were reduced by factors of five and two, respectively, while the final Nb concentration was larger. These differences can be attributed to the different melting temperatures and different phase diagrams corresponding to these materials.

2.2. SPVD method

Zirconia is a high-temperature material, and therefore, the evaporation temperature for zirconia in the Heliotron reactor is estimated to be about 3000 °C. Such temperatures are achieved with heat transfer via concentration of solar radiation focused to small spot sizes. The estimated maximal power density can reach up to 5 kW/cm^2. The schematic of the SPVD method is shown in Fig. 1 along with the evaporation process in Fig. 2.

The mobile plane mirrors follow the movement of the sun and reflect solar radiation onto the parabolic mirror, whose emission is concentrated on the sample with spot sizes below 1 cm^2. For power control, the flaps between the mobile plane mirrors and the parabolic mirror are used. The target material is placed at the focus of the parabolic mirror in a water-cooled target holder, which is placed at the center of the glass balloon of the reactor. This setup facilitates variation of the ambient gas and gas pressure while also allowing gas flow for controlled material transport. The evaporated particles are transported by gas flow along the cooling part (the cold finger) to nanoporous ceramic filters. Such particle transport reduces the particle condensation on the walls and allows controlled particle collection at the filters. The power density, gas type, pressure, and flow rate in the reactor also affect the properties of the prepared samples.

2.3. Morphology and structure measurements

Energy dispersive X-ray (EDX) analysis of the samples (using the Eagle III XPL) was carried out for controlling the dopant content and detecting unexpected impurities. The crystalline structure of the samples was examined via X-ray diffraction (XRD) using an X-ray diffractometer (X'Pert Pro MPD) with Cu Kα radiation (λ = 0.154 nm). The crystalline size verification and morphology studies were performed using a transmission electron microscope (TEM, Tecnai G20, FEI) operated at 200 kV. An ultrasonic bath was used for powder treatment. Sol Gel samples when mixed in ethanol undergo partial precipitation, thereby indicating the presence of large agglomerations of the particles, whereas the SPVD samples remain milky; in this manner, the difference in terms of agglomeration between samples obtained by the two methods can be compared. The samples for TEM studies were placed on a carbon-coated grid. For verification of the dopant incorporation in nanocrystals, we performed STEM observations with an EDX detector.

2.4. Optical measurements

The luminescence measurements were carried out at room temperature. The luminescence measurements were carried out using three different excitation sources: (I) YAG laser FQSS266 (CryLas

Table 1
Sample names used in text with corresponding structure, grain sizes, doping content, and annealing temperatures.

Sample name	Structure	Grain sizes (nm)		Dopands (mol%)			Annealing T (°C)
		M	T	Er	Yb	Nb	
Sol Gel 12-8	T	–	–	1	2	3	1000
Sol Gel 12-10	T	–	–	1	2	0	1000
SPVD 12-8	T	–	21–22	0.2	1.12	4.4	None
SPVD 12-10	T	–	15–17	0.22	1.18	0	None
Sol Gel 13-8a	T65% + M35%	35–40	20	0.2	1.12	4.4	800
Sol Gel 13-8b	M68% + T32%	40–45	35	0.2	1.12	4.4	1000

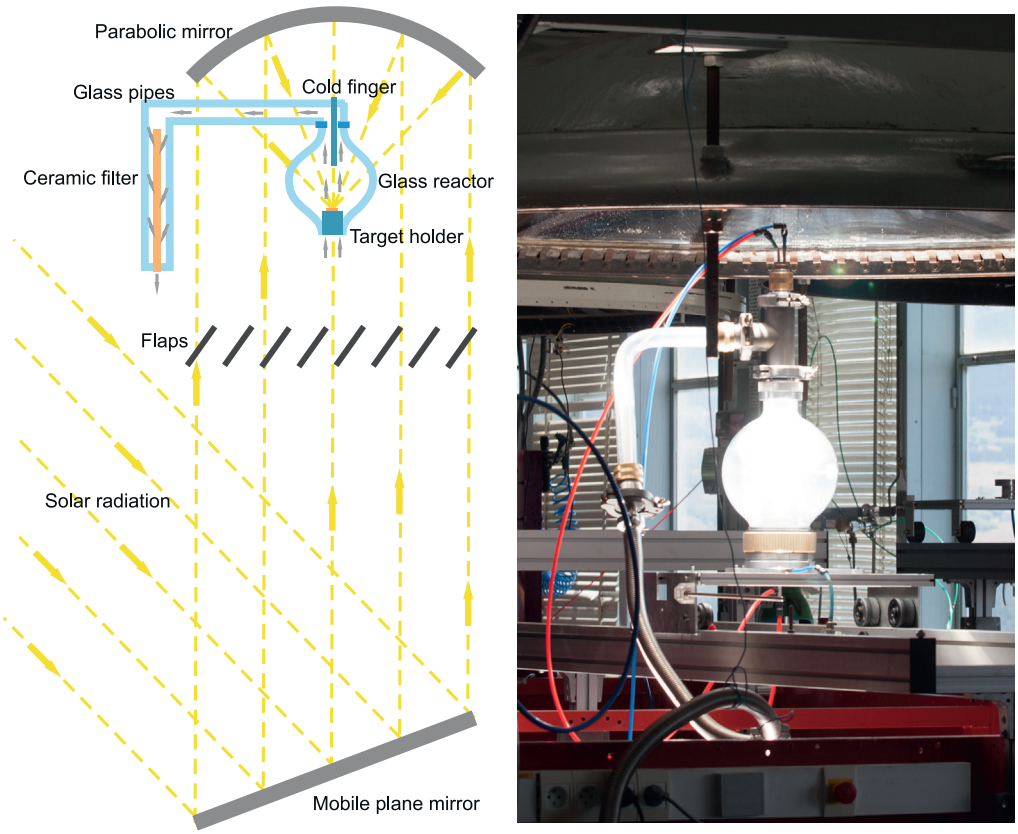

Fig. 1. Schematic of Heliotron reactor (left panel) and its photograph (right panel).

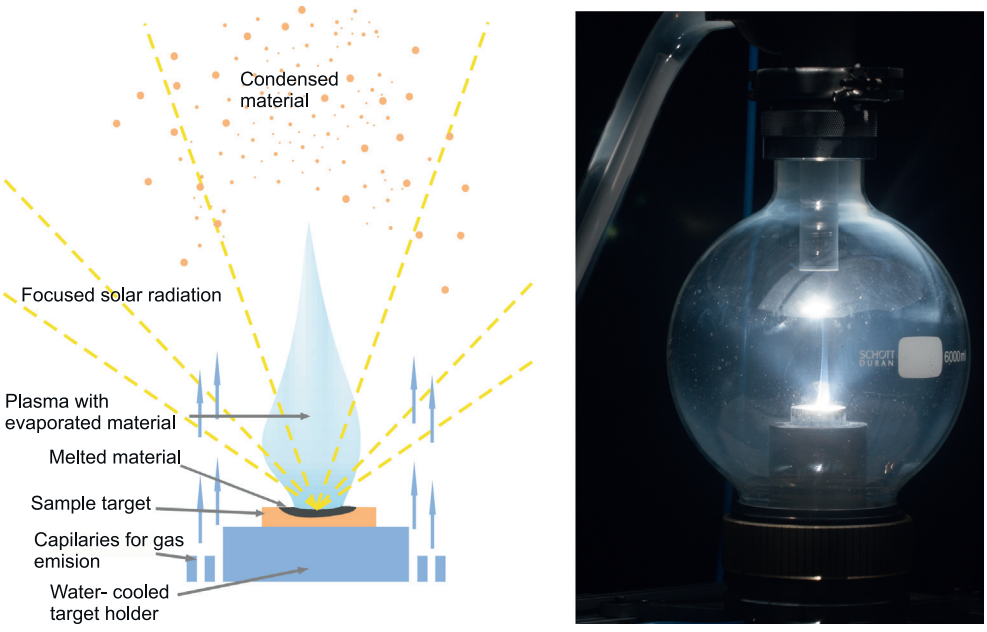

Fig. 2. Schematic of plasma evaporation process inside Heliotron reactor (left panel) and photograph of reactor (right panel).

GmbH), fourth harmonic, 266 nm (4.66 eV), 2-ns pulses, (II) a 975-nm Thorlabs L975P1WJ laser diode coupled with a Thorlabs ITC4005 controller, and (III) X-ray tube with a tungsten anode operated at 30 kV, 15 mA. The samples for luminescence measurements were pressed into similar-sized tablets, and therefore, the geometries of the excitation–registration channels were mostly identical. Consequently, comparison of the luminescence intensities from the samples was made possible.

The luminescence spectra were recorded using the Andor Shamrock B-303i spectrograph equipped with a CCD camera (Andor DU-401A-BV). All luminescence measurements were obtained at room temperature.

3. Results and discussion

The SPVD-prepared zirconia nanocrystals contain relatively small quantities of Er and Yb when compared with the quantities in the target material. The zirconia nanocrystal structure dependence on the Er concentration has been previously shown by Lai et al., who have reported that the metastable tetragonal phase becomes dominant for samples with Er-ion concentrations over 4 mol% [17]. The XRD data indicate that for the Sol Gel samples, a mixture of tetragonal and monoclinic phases is present, and for SPVD samples, only the tetragonal phase is present (Fig. 3). The stable tetragonal phase is due to the small nanocrystal sizes. Such tetragonal phase stabilization has been described by Garvie et al., who showed that for nanocrystals with sizes below 30 nm, the tetragonal phase is stabilized via excess surface energy [18]. Annealing of the Sol Gel samples at 1000 °C leads to increase in the grain size and further increase in the monoclinic-phase quantity in the mixture.

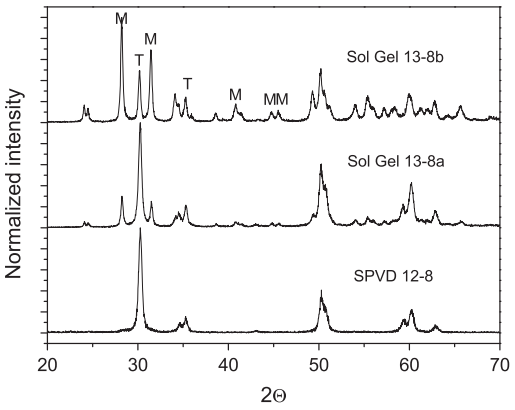

Fig. 3. X-ray diffraction patterns of Sol Gel and SPVD samples. The monoclinic phase reflex peaks are indicated by the letter M and those of the tetragonal phase are indicated by the letter T. Here, sample 13-8a was annealed at 800 °C, whereas sample 13-8b was annealed at 1000 °C.

The actual amounts of Er, Yb, and Nb in the samples were estimated via EDX analysis. The descriptions of the samples examined are listed in Table 1.

As described in our previous research on ZnO, the SPVD samples show a very different morphology in comparison with the Sol Gel samples; in this light, we studied the SPVD-prepared ZrO_2 morphology. The STEM image studies showed that the Sol Gel samples mostly form agglomerates while the SPVD samples consist of fine separate particles (Fig. 4). Particle agglomeration is very common problem in the synthesis of zirconia nanoparticles [19–21]; however, in the light of biolabeling applications, nanocrystal synthesis with small sizes and without agglomeration is necessary.

The SPVD samples exhibit a very well-formed crystalline structure (Fig. 5), whereas in the Sol Gel samples, the crystal structure is less pronounced. This could be related to the presence of an amorphous layer on the grain boundaries and also considerably larger defect concentrations. The SPVD samples exhibited a very fine crystal structure even for particles with sizes below 5 nm.

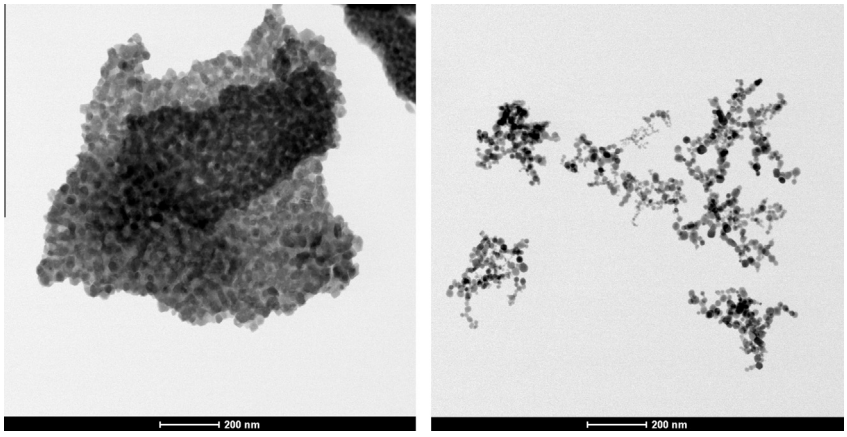

Fig. 4. Typical STEM-image representations of Sol Gel 13-8a (left panel) and SPVD 12-8 powder (right panel) samples.

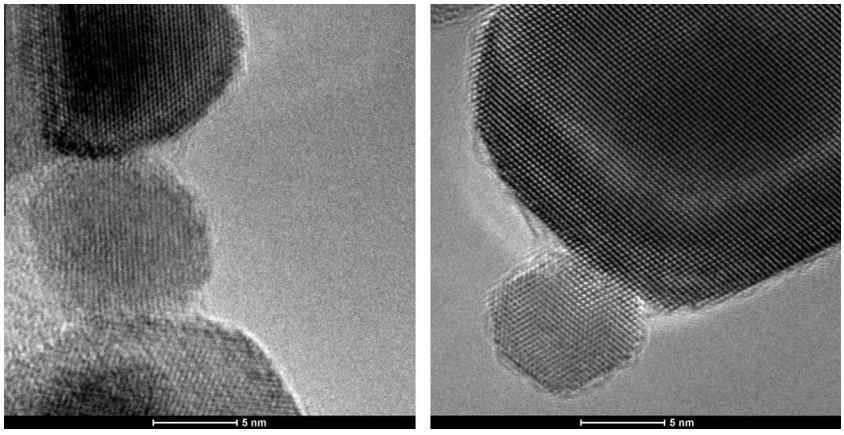

Fig. 5. High-resolution TEM images of zirconia nanoparticles prepared with Sol Gel (left panel) and SPVD (right panel) methods.

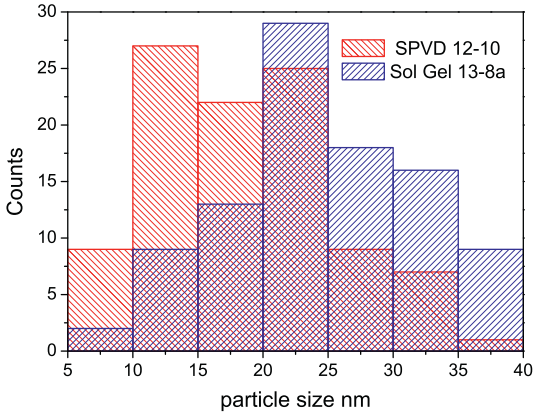

Fig. 6. Particle size distribution for two samples with the same dopant content prepared by the Sol Gel and SPVD methods. Sizes were estimated from STEM images (statistic from 100 particles).

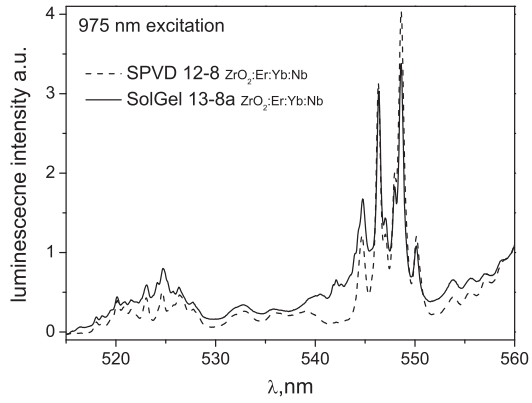

Fig. 7. Upconversion luminescence for Sol Gel 13-8a and SPVD 12-8 samples excited at 975 nm.

The average particle size distribution for the SPVD samples lies mostly in the range of 10–25 nm, whereas for Sol Gel samples, this distribution is somewhat broader and is in the 15–35-nm range (Fig. 6). We speculate that in the SPVD process, while there are larger amounts of particles with sizes below 10 nm directly after condensation, a fraction of these particles is lost due to insufficient carrier gas filtration. This is also one explanation as to why the fraction of particles with sizes above 10 nm is so large.

The upconversion luminescence intensities for samples obtained with SPVD and Sol Gel methods excited at 975 nm are similar, whereas the spectral distribution differs between the two cases (Fig. 7). The SPVD sample exhibits more luminous intensity from the $^4S_{3/2} \rightarrow {}^4J_{15/2}$ transition with the main peak at 549 nm, whereas the Sol Gel sample shows more intense bands corresponding to the $^2H_{11/2} \rightarrow {}^4J_{15/2}$ transition in 540–545-nm range. The luminescence in this range originates from the Er ions associated with oxygen-vacancy-related defects [8].

The luminescence intensity for zirconia nanocrystals increases with increase in grain size [8,22]; however, the upconverted luminescence intensities of the SPVD and Sol Gel samples are similar, thereby indicating that in Sol Gel samples, the defect concentration is also larger.

In the case of zirconia doped with Er and Yb (without Nb), the Er-ion luminescence was relatively weak in both the SPVD and Sol Gel samples. The Nb doping reduces the oxygen-vacancy concentration [13], thereby reducing the defect luminescence and strongly increasing the Er doping luminescence [9]. The same phenomenon was observed for SPVD samples also. To illustrate

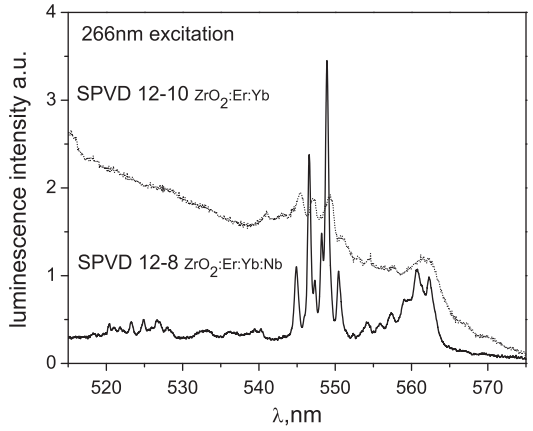

Fig. 8. Luminescence spectra for SPVD 12-8 and SPVD 12-10 samples.

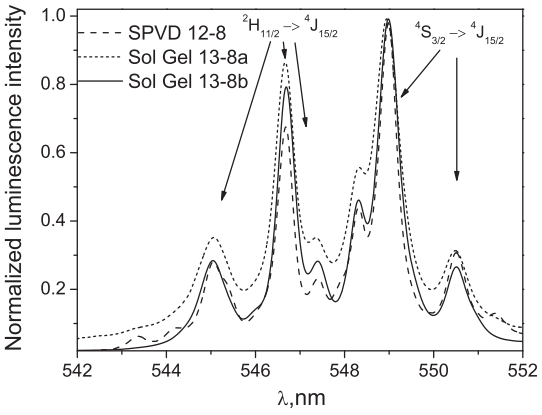

Fig. 9. Normalized upconversion luminescence intensity for particle excitation at 975 nm.

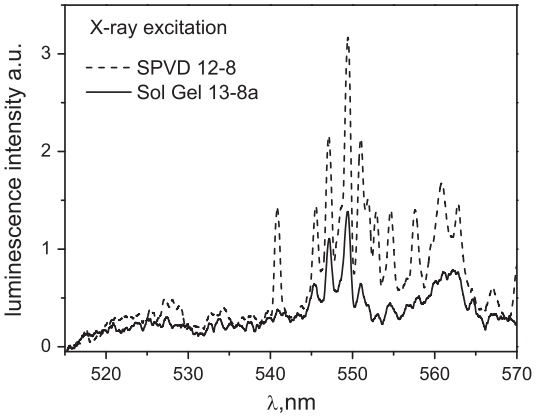

Fig. 10. X-ray-excited luminescence spectra for SPVD 12-8 and Sol Gel 13-8a samples.

this effect, a 266-nm laser was used to illuminate samples in which no Nb was added. A broad luminescence band related to the intrinsic defects in zirconia was dominant, and upon adding Nb, the defect luminescence band was strongly suppressed and the Er-ion luminescence bands increased (Fig. 8).

Despite Nb doping, the Sol Gel samples still exhibit Er-ion bands that are associated with oxygen-vacancy-related defects at 545 and 546.5 nm (Fig. 9). This could be related to the nature of nanocrystal formation. In the Sol Gel method, crystal growth occurs at

relatively low temperatures, whereas in SPVD, crystals are formed from the vapor phase.

This difference in the nature of crystal formation was verified by using a Sol Gel sample annealed at 1000 °C. With increase in annealing temperature, the grain size increased to ~40 nm, and the luminescence intensity increased by a factor of 10. Further, the Er bands associated with the defects decreased, and the spectral distribution was closer to that of the SPVD sample.

Further evidence of the larger concentration of defects in Sol Gel nanocrystals is provided by the fact that the SPVD samples exhibit stronger luminescence intensity peaks (Fig. 10). Thus, we can conclude that in the case of SPVD, the energy transfer from the host matrix to Er ions is more efficient than in Sol Gel nanocrystals. The energy transfer in Sol Gel samples could be suppressed by defects.

4. Conclusions

Our study reports the vapor deposition of zirconia to realize nanoparticle preparation.

These synthesized nanocrystals showed less agglomeration and better crystallinity.

The luminescence intensity of the SPVD particles was close to that of particles synthesized via the Sol Gel method, thereby indicating that both methods can be utilized for luminescent-particle synthesis; however, for applications such as biolabeling in which non-agglomerated particles are necessary, the SPVD method is more appropriate.

The luminescence spectral distributions for Sol Gel and SPVD samples are different, and these differences are related to the defects present in the Sol Gel samples. Some differences in the spectral distributions are related to presence of oxygen vacancies.

Annealing of the Sol Gel samples at temperatures of 1000 °C strongly increased the luminescence intensity and reduced the defect concentration; however, this annealing resulted in large grain sizes.

We believe that our approach can significantly contribute to the use of zirconia nanocrystals in biolabeling applications.

Acknowledgments

This work was supported by grants from the Latvian Council of Science (Grants 2013.10-5/014 (LZP N 302/2012)). The sample preparation was carried out under the aegis of the SFERA Grant Agreement No. 22829. The authors are grateful to Aija Krumina and Dr. L. Skuja for XRD data and energy dispersive X-ray analysis of the samples.

References

[1] N. Maeda, N. Wada, H. Onoda, A. Maegawa, K. Kojima, Spectroscopic properties of Er^{3+} in sol–gel derived ZrO_2 films, Thin Solid Films 445 (2003) 382–386.
[2] K. Smits, L. Grigorjeva, D. Millers, A. Sarakovskis, A. Opalinska, J.D. Fidelus, W. Lojkowski, Europium doped zirconia luminescence, Opt. Mater. 32 (2010) 827–831.
[3] L. Huangqing, W. Lingling, C. Shuguang, Z. Bingsuo, P. Zhiwei, Effect of annealing temperature on luminescence of Eu^{3+} ions doped nanocrystal zirconia, Appl. Surf. Sci. 253 (2007) 3872–3876.
[4] K. Smits, J. Liepins, M. Gavare, A. Patmalnieks, A. Gruduls, D. Jankovica, Zirconia nanocrystals as submicron level biological label, IOP Conf. Ser. Mater. Sci. Eng. 38 (2012) 012050.
[5] G.Y. Chen, Y.G. Zhang, G. Somesfalean, Z.G. Zhang, Q. Sun, F.P. Wang, Two-color upconversion in rare-earth-ion-doped ZrO_2 nanocrystals, App. Phys. Lett. 89 (2006) 163105.
[6] K. Smits, L. Grigorjeva, D. Millers, A. Sarakovskis, J. Grabis, W. Lojkowski, Intrinsic defect related luminescence in ZrO_2, J. Lumin. 131 (2011) 2058–2062.
[7] L. Grigorjeva, D. Millers, K. Smits, V. Pankratov, W. Łojkowski, J. Fidelus, T. Chudoba, K. Bienkowski, C. Monty, Excitonic luminescence in ZnO nanopowders and ceramics, Opt. Mater. 31 (2009) 1825–1827.
[8] K. Smits, D. Jankovica, A. Sarakovskis, D. Millers, Up-conversion luminescence dependence on structure in zirconia nanocrystals, Opt. Mater. 35 (2013) 462–466.
[9] K. Smits, A. Sarakovskis, L. Grigorjeva, D. Millers, J. Grabis, The role of Nb in intensity increase of Er ion upconversion luminescence in zirconia, J. Appl. Phys 115 (2014) 213520, http://dx.doi.org/10.1063/1.4882262.
[10] S. Fabris, A.T. Paxton, M.W. Finnis, A stabilization mechanism of zirconia based on oxygen vacancies only, Acta Mater. 50 (2002) 5171–5178.
[11] X. Guo, Effect of Nb_2O_5 on the space-charge conduction of Y_2O_3-stabilized ZrO_2, Solid State Ionics 99 (1997) 137–142.
[12] D. Kim, H.-J. Jung, D.-H. Cho, Phase transformations of Y_2O_3 and Nb_2O_5 doped tetragonal zirconia during low temperature aging in air, Solid State Ionics 80 (1995) 67–73.
[13] Z. Wang, Z.Q. Chen, J. Zhu, S.J. Wang, X. Guo, Evidence of defect associates in yttrium-stabilized zirconia, Radiat. Phys. Chem. 58 (2000) 697–701.
[14] D.G. Lamas, G.E. Lascalea, N.E. Walsoe de Reca, Synthesis and characterization of nanocrystalline powders for partially stabilized zirconia ceramics, J. Eur. Ceram. Soc. 18 (1998) 1217–1221.
[15] K.A. Singh, L.C. Pathak, S.K. Roy, Effect of citric acid on the synthesis of nanocrystalline yttria stabilized zirconia powders by nitrate-citrate process, Ceram. Int. 33 (2007) 1463–1468.
[16] J. Kouam, T. Ait-Ahcene, A.G. Plaiasu, M. Abrudeanu, A. Motoc, E. Beche, C. Monty, Characterization and properties of ZnO based nanopowders prepared by solar physical vapor deposition (SPVD), Sol. Energy 82 (2008) 226–238.
[17] L.-J. Lai, T.-C. Chu, M.-I. Lin, Y.-K. Lin, Photoluminescence of thin films ZrO_2: Er^{3+} excited by soft X-ray, Solid State Commun. 144 (2007) 181–184.
[18] R.C. Garvie, The occurrence of metastable tetragonal zirconia as a crystallite size effect, J. Phys. Chem. 69 (1965) 1238–1243.
[19] R. Ahmad, J.-H. Ha, I.-H. Song, Effect of valeric acid on the agglomeration of zirconia particles and effects of the sintering temperature on the strut wall thickness of particle-stabilized foam, J. Eur. Ceram. Soc. 34 (2014) 1303–1310.
[20] F. Davar, M.R. Loghman-Estarki, Synthesis and optical properties of pure monoclinic zirconia nanosheets by a new precursor, Ceram. Int. 40 (2014) 8427–8433.
[21] Z. Hua, X.M. Wang, P. Xiao, J. Shi, Solvent effect on microstructure of yttria-stabilized zirconia (YSZ) particles in solvothermal synthesis, J. Eur. Ceram. Soc. 26 (2006) 2257–2264.
[22] A. Patra, C.S. Friend, R. Kapoor, P.N. Prasad, Effect of crystal nature on upconversion luminescence in Er^{3+}: ZrO_2 nanocrystals, Appl. Phys. Lett. 83 (2003) 284–286.